Integration and Execution of Community Land Model Urban (CLMU) in a Containerized Environment

Junjie Yu[1], Yuan Sun[1], Sarah Lindley[2], Caroline Jay[3], David O. Topping[1], Keith Oleson[4], Zhonghua Zheng[1*]

[1*]Department of Earth and Environmental Sciences, The University of Manchester, Manchester, M13 9PL, UK.
[2]Department of Geography, The University of Manchester, Manchester, M13 9PL, UK.
[3]Department of Computer Science, The University of Manchester, Manchester, M13 9PL, UK.
[4]Climate and Global Dynamics Laboratory, NSF National Center for Atmospheric Research (NSF NCAR), Boulder, CO 80307, USA.

*Corresponding author(s). E-mail(s):
zhonghua.zheng@manchester.ac.uk;
Contributing authors: junjie.yu@postgrad.manchester.ac.uk;
yuan.sun-7@postgrad.manchester.ac.uk;
sarah.lindley@manchester.ac.uk; caroline.jay@manchester.ac.uk;
david.topping@manchester.ac.uk; oleson@ucar.edu;

Abstract

The Community Land Model Urban (CLMU) is a process-based numerical urban climate model that simulates the interactions between the atmosphere and urban surfaces, serving as a powerful tool for the convergence of urban and climate science research. Despite its advanced capabilities, CLMU presents significant challenges for users unfamiliar with numerical modeling due to the complexities of model installation, environment and case configuration, and generating model inputs. To address these challenges, a toolkit was developed, including (1) an operating system-independent containerized application developed to streamline the execution of CLMU and (2) a Python-based tool (Pyclmuapp) used to interface the containerized CLMU and create urban surface data and atmospheric forcing data for the model. This toolkit enables users to simulate urban climate

and explore climate-related variables such as urban building energy consumption, urban water balance, and human thermal stress. It also supports the simulation under future climate conditions and the exploration of urban climate responses to various surface properties, providing a foundation for evaluating urban climate adaptation strategies. Overall, this toolkit makes urban climate modeling more accessible, promoting broader applications from research to practical urban planning and policy-making.

Keywords: Urban climate modeling, Containerized application, Climate change, Urban climate

1 Introduction

Urban areas constitute only 0.2%–3% of the Earth's land surface (Potere & Schneider, 2007; Schneider, Friedl, & Potere, 2009), yet they are home to more than 50% of the population (Ritchie, Samborska, & Roser, 2024) and account for about 70% of greenhouse gas emissions ("Urban Systems and Other Settlements", 2023). Urbanization changes the land surface and increases anthropogenic heat emissions, thus inducing variations in urban climate (Dimoudi et al., 2013; Shahrestani et al., 2015). One of the critical variations is the urban heat island (UHI) effect, where urban areas retain more heat than the surrounding areas (D. Li et al., 2024). Such variations often pose a greater risk of extreme climates (J. Wang et al., 2021; Zheng, Zhao, & Oleson, 2021), posing the urban economy (Yin et al., 2023), residents' health (Hu et al., 2023), and critical infrastructure (Dodman et al., 2022) to high-risk conditions. These impacts have resulted in numerous studies revolving around the urban climate from technological advancements to societal implications (Adilkhanova, Santamouris, & Yun, 2024; Anderson et al., 2018; Ghanbari et al., 2023; J. Wang et al., 2021; Zhao et al., 2021).

Urban and climate science convergence research often benefits from urban climate models. These numerical models, built upon physical processes (Grimmond et al., 2009; M.J. Lipson et al., 2024; Oke et al., 2017a), primarily describe the interaction of the urban surface with the atmosphere (Oke et al., 2017b), including the impacts of changing surface properties and anthropogenic emissions. Changes in urban properties such as cover types, quantities, materials, and structures are linked to urban form, and changes in emissions are associated with urban function, and both serve as important components of urban design and planning (Oke et al., 2017b). The associated interconnections provide the core rationale for urban planning guided by urban climate modeling. For instance, supported by these models, city authorities can effectively plan and implement strategies to mitigate urban heat island effects, reduce flood risks, and enhance climate resilience in urban areas (Dodman et al., 2022).

The Community Land Model Urban (CLMU), integrated for urban climate and surface energy simulations within the Community Land Model (CLM) of the Community Earth System Model (CESM) (K. Oleson et al., 2010), is the only model in the Coupled Model Intercomparison Project Phase 5 (CMIP5) that provides physics-based urban simulations (Zhao et al., 2021). In recent years, the CLMU has played

an active role in the urban climate research community, contributing to understanding mechanisms such as the UHI effect (C. Li et al., 2024; Lyu et al., 2024) and humid heat (Zhang et al., 2023). It has also been used to project future urban temperatures (Zhao et al., 2021), heatwaves (Zheng et al., 2021) and humid heat (Yang, Zhao, & Oleson, 2023), as well as to evaluate the effects of urban adaptation strategies (L. Wang, Huang, & Li, 2020). Table 1 highlights some of the CLMU's contributions to the scientific community over the past five years.

Table 1 CLMU application for the scientific community

Theme	CLMU's contributions	Ref
Spatial patterns and mechanism of UHI	Air temperature UHI analysis	Lyu et al. (2024)
Mechanism of UHI	Biophysical analysis of UHI	C. Li et al. (2024)
Mechanism of humid heat	Urban humid heat modeling	Zhang et al. (2023)
Projection of humid heat and adaptation	Urban temperature and humidity modeling	Yang et al. (2023)
Spatial and temporal patterns of urban canopy air temperature to anthropogenic heat flux	Urban canopy air temperature and anthropogenic heat flux modeling	L. Wang et al. (2023)
Correlated analysis of UHI/heat index and climate dynamics and energy budget	UHI and heat index modeling	Mohammad Harmay and Choi (2023)
Modeling of UHI and thermal comfort during heat wave	UHI and thermal comfort modeling	C. Li et al. (2023)
Analysis of climate change on global total and urban runoff	Urban runoff modeling	Gray, Zhao, and Stillwell (2023)
Projection of urban heat wave	Urban temperature modeling	Zheng et al. (2021)
Projection of urban temperature and humidity	Urban temperature and humidity modeling	Zhao et al. (2021)
Mechanism of UHI	Urban heat island analysis	C. Li and Zhang (2021)
Evaluation of adaption strategies	Evaluation of the effectiveness of implementing white roofs	L. Wang et al. (2020)

However, using the CLMU presents three major challenges for those unfamiliar with numerical modeling. (a) The model installation is particularly complex. As a numerical model written in Fortran, CLMU requires several supporting software packages and is limited to UNIX-style operating systems, making it difficult for users of non-UNIX operating systems. The prerequisites of specific software/dependencies versions can make installation cumbersome. Users often need to reconfigure their system to accommodate the model, which adds to complexity. (b) The simulation case configuration (for running the model) is intricate. Users must be familiar with machine configuration and environment settings, a process that could be tedious and prone to debugging issues. (c) Running the model requires various urban surface data and atmospheric forcing data, which can be particularly challenging for users unfamiliar with weather/climate-related numerical simulations. Overall, these obstacles collectively deter users (e.g., urban climate researchers, educational institutions, and stakeholders from local authorities (Nilsen et al., 2022)) from easily operating CLMU, potentially excluding a wide range of users who could benefit from its capabilities. To promote

the practical application of urban climate modeling in areas such as urban planning and policy analysis, a more accessible simulation toolkit is necessary.

The objective of this study is to develop a toolkit for executing CLMU that addresses the aforementioned challenges. The toolkit includes the containerized version of CLMU (CLMU-App) and the Python tool (Pyclmuapp) that interacts with CLMU-App. The structure of this study is organized as follows. Section 2 provides an overview of CLMU. Section 3 presents CLMU-App, which was developed to simplify installation and environment configuration. Section 4 introduces Pyclmuapp, which facilitates the creation of urban surface and atmospheric forcing data, as well as the execution of simulations and customization of scenarios, addressing the challenge of users lacking input data. Section 5 demonstrates the potential applications of Pyclmuapp by use cases. The final section summarizes the implications, limitations, and future work.

2 Overview of CLMU

CLMU is a process-based numerical model for simulating urban climate and has been implemented as part of the Community Land Model (CLM) within the Community Earth System Model (CESM) (K.W. Oleson & Feddema, 2020; Zhao et al., 2021). Other Earth System Models (ESMs) also benefit from CLMU, including E3SM (USA) (Golaz et al., 2019), CMCC-ESM2 (Italy) (Lovato et al., 2022), FGOALS-f3-H/FGOALS-f3-L (China) (Bao et al., 2020) and NorESM (Norway) (Seland et al., 2020). Fig. 1 illustrates the CESM subgrid hierarchy and the CLMU canyon model schematic. In CLMU, urban surfaces interact with the atmospheric forcing variables, either from prescribed data or through an online atmospheric model, to simulate past, present, and future climates. While CLMU focuses on simulating urban landunits, its host model, CLM, also supports other land types, such as vegetation, lakes, crops, and even glaciers (Fig. 1). Notably, in the current version of CLM, CLMU does not interact with other landunits, which is why it can be treated as a standalone component.

CLMU models the urban area as an "urban canyon", characterized by building height and street width Oke (1987). Within the urban surfaces ("urban columns" in CLMU modeling)–roof, walls (both shaded and sunlit), and canyon floor (impervious and pervious roads)–each is modeled to compute turbulent fluxes. The model also accounts for complex processes such as radiation trapping within the urban canyon, heat conduction and convection across the urban columns, and roof and canyon floor (impervious and pervious) hydrological processes, providing insights into urban heat and water transfer. Furthermore, it integrates a building energy model (BEM) that accounts for heat conduction, convection, and ventilation of buildings, as well as anthropogenic heat sources from heating and air conditioning systems (HAC). With the urban parameterization (using parameters to describe the urban surface properties), CLMU can compute the energy and turbulent fluxes, and climate-related variables with the forcing from the atmosphere model or observational data. More details of CLMU can be found in K. Oleson et al. (2010), and the details of the BEM in CLMU are described in K.W. Oleson and Feddema (2020). It should be noted that in the current version of CLMU, vegetation is not explicitly considered. Instead, a pervious canyon floor is used to approximate evaporation from vegetated surfaces.

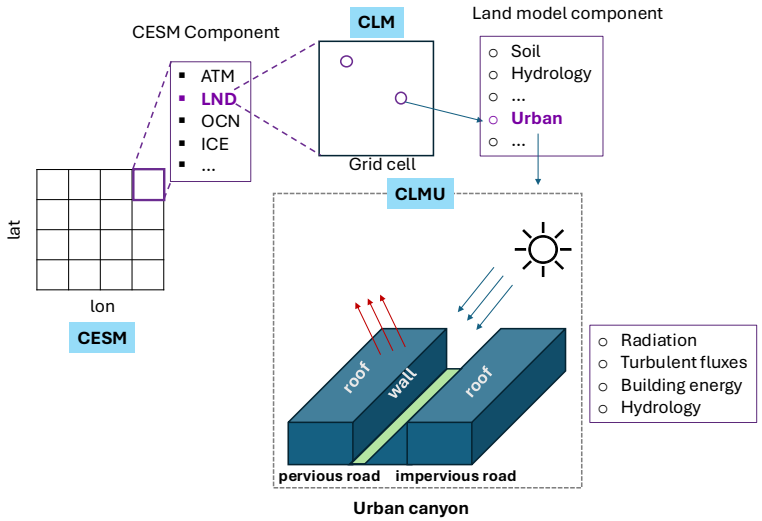

Fig. 1 CESM subgrid hierarchy and CLMU canyon model. ATM: atmosphere model. LND: land model. OCN: ocean model. ICE: sea ice model.

By providing atmospheric forcing data and urban surface input data, CLMU can model the climate in the urban canyon. The model time-step is 1800 seconds, which is sufficient for resolving the diurnal cycle.

CLMU simulations have been validated by both in-situ and remote sensing observations (Demuzere et al., 2017; Fitria et al., 2019; Mohammad Harmay & Choi, 2023; Zhao et al., 2014, 2021). Zhao et al. (2021) further evaluated the capacity of CLMU in climate modeling, showing that CLMU reproduces the daily distributions of urban climate, including maximum, minimum, and mean air temperature, through comparisons with the observational dataset (PRISM) and Weather Research & Forecasting Model (WRF) simulations. The results of CLMU and WRF models demonstrate good consistency in both magnitude and spatial variation of the projected urban warming signals. Furthermore, in Urban-PLUMBER, a community-based project for urban climate model intercomparisons focusing on local-scales (order 0.1–5 km) energy exchange between the urban surface and the atmosphere (M.J. Lipson et al., 2024), CLMU demonstrated its ability to produce accurate urban climate responses and offer a relative variety of output variables (experiment details are available at https://urban-plumber.github.io/AU-Preston/plots/). These results highlight the effectiveness of CLMU in urban climate modeling.

3 CLMU in a Containerized Environment

Concerning the complexities of installation and environment configuration, we employ containerization, which packages code and all its dependencies into a standardized software unit, enabling applications to run efficiently and reliably from one computing

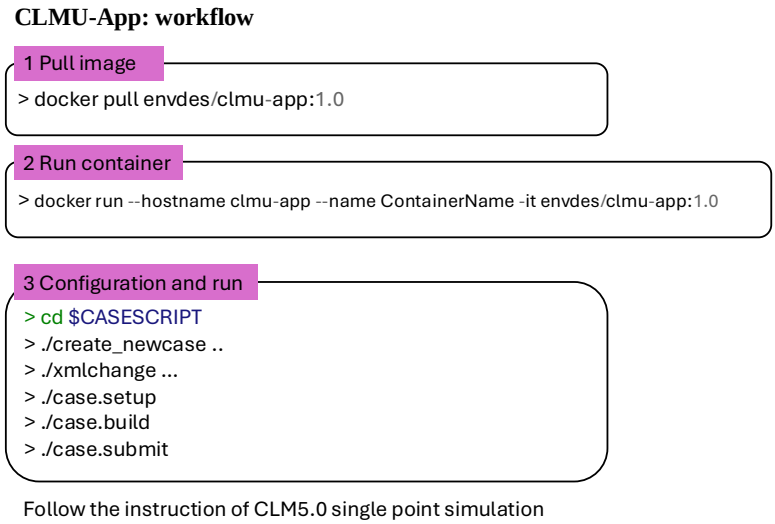

Fig. 2 Workflow of running CLMU simulations using CLMU-App.

environment to another. This approach can make the model run the same way regardless of the underlying infrastructure, such as Windows or Linux operating systems. Here, we developed CLMU-App, a Docker container image that includes everything needed to run a CLMU simulation. This image becomes a container when executed on a container runtime, such as the Docker Engine. By easily pulling this containerized application image to their local machine, users only need to know how to run the CLM case without installation and configuration repeatedly and it can be used on demand. The structure of CLMU-App is shown in the left panel of Fig. 3. The current version is built on Fedora 31 (a Linux distribution version), with the major dependencies of GCC 9.3.1 (compiler), Cmake 3.18, NetCDF-C 4.7.0-2, NetCDF-Fortran 4.5.2-3, Python 3.7.9, SVN 1.12 and ESMF 8.0. To make the image available on AMD 64 and ARM 64 platforms, the "buildx" (a Docker command line interface (CLI) plugin for extended build capabilities with BuildKit) was applied to build up AMD 64 and ARM 64 images. The CLM release tag is "release-clm5.0.37-1-ge7285f6ca", which is a stable version of the released CLM 5.0. This container image is open-source and available on DockerHub (https://hub.docker.com/r/envdes/clmu-app). For high-performance computing (HPC) users, the container can be converted to run on Singularity/Apptainer, a container platform similar to Docker.

The following diagram outlines the steps required to use CLMU-App for simulations. After installing Docker, the next step is to pull the image, followed by running the container. The container should be run using the image with a specific hostname (clmu-app). The subsequent steps involve configuration and execution, following the same process as a typical CLM single point case. Users can refer to ClMU-App document (https://envdes.github.io/clmu-app/) for the details of application details and instruction.

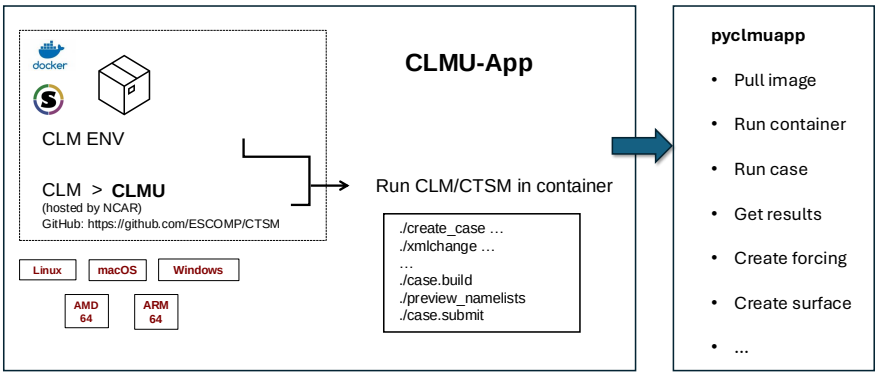

Fig. 3 Structure of CLMU-App and Pyclmuapp.

4 Pyclmuapp: A Python package to interact with CLMU-App

The Pyclmuapp interacts with the CLMU-App with Python functions including running a container, configuring simulation cases, modifying urban surface and atmospheric forcing data, creating urban surface and atmospheric forcing input of the selected point, and retrieving simulation results (right panel of Fig. 3). In this version of CLMU, each urban column is parameterized with radiative, morphological, and thermal variables. The modifiable urban parameters in surface input data are listed in Table 2.

Running a global case requires substantial computing resources, often making execution impractical on personal machines. Consequently, Pyclmuapp is designed exclusively for single-point simulations (running one select grid cell of interest with provided surface data at a time) and is not recommended for global-scale simulations. The single-point simulations model a grid cell that contains urban landunit and other landunits. The area of urban does not affect the urban climate in CLMU single-point simulations as the urban landunit is not interacting with others. One significant advantage of single-point simulations is the reduced computational load, making the simulations more accessible and affordable for all users. Additionally, the lower cost enables a wide range of explorations, such as studying the impact of changes in urban surfaces or atmospheric forcing data on urban climates. These explorations are crucial for urban planning and adaptation to changing climates, broadening the application of urban climate modeling across multiple disciplines. Notably, the soil texture of urban surface parameters is only used to describe the soil beneath the impervious canyon floor and the pervious canyon floor soil.

4.1 User-defined single-point simulation

In user-defined single-point simulation, the atmospheric forcing data and surface data are provided by the users. In this mode, users can manually specify the available

Table 2 Urban surface parameters for CLMU modeling

Variable	Long name	Units	Category	Modifiable
ALB_ROOF_DIR	Direct albedo of roof	Unitless	Radiative	Y
ALB_WALL_DIR	Direct albedo of wall	Unitless	Radiative	Y
ALB_IMPROAD_DIR	Direct albedo of impervious road	Unitless	Radiative	Y
ALB_ROOF_DIF	Diffuse albedo of roof	Unitless	Radiative	Y
ALB_WALL_DIF	Diffuse albedo of wall	Unitless	Radiative	Y
ALB_IMPROAD_DIF	Diffuse albedo of impervious road	Unitless	Radiative	Y
EM_ROOF	Emissivity of roof	Unitless	Radiative	Y
EM_WALL	Emissivity of wall	Unitless	Radiative	Y
EM_IMPROAD	Emissivity of impervious road	Unitless	Radiative	Y
CANYON_HWR	Canyon height to width ratio	Unitless	Morphological	Y
HT_ROOF	Height of roof	Meters	Morphological	Y
THICK_ROOF	Thickness of roof	Meters	Morphological	Y
THICK_WALL	Thickness of wall	Meters	Morphological	Y
WTLUNIT_ROOF	Fraction of roof	Unitless	Morphological	Y
WTROAD_PERV	Fraction of pervious road	Unitless	Morphological	Y
WIND_HGT_CANYON	Height of wind in canyon	Meters	Morphological	Y
TK_ROOF	Thermal conductivity of roof	W/m*K	Thermal	Y
TK_WALL	Thermal conductivity of wall	W/m*K	Thermal	Y
TK_IMPROAD	Thermal conductivity of impervious road	W/m*K	Thermal	Y
CV_ROOF	Volumetric heat capacity of roof	J/m^3*K	Thermal	Y
CV_WALL	Volumetric heat capacity of wall	J/m^3*K	Thermal	Y
CV_IMPROAD	Volumetric heat capacity of impervious road	J/m^3*K	Thermal	Y
T_BUILDING_MIN	Minimum interior building temperature	Kelvin	Indoor	Y
T_BUILDING_MAX	Maximum interior building temperature	Kelvin	Indoor	N
PCT_SAND	Percent sand of pervious road (soil)	Unitless	Soil texture	N
PCT_CLAY	Percent clay of pervious road (soil)	Unitless	Soil texture	N

Y indicates the variable can be modified by Pyclmuapp. N indicates the variable can not be directly modified by the current version of Pyclmuapp but can be further revised by users.

urban surface and atmospheric forcing input files. The advantage of this mode is that the amount of input data required is lightweight because the urban surface and atmospheric forcing data are all single-point files. Similarly, manual modification of the urban surface and atmospheric forcing data can be performed to simulate the potential impacts of urban planning and design, and future climate change on the urban climate, e.g., modifying the roof height to simulate the effect of building height on urban climates.

The accompanying illustration depicts the workflow for executing CLMU simulations with the pyclmuapp tool, comprising four distinct phases (Fig. 4). The initialization phase is the first step in the workflow. The Pyclmuapp should be imported and a 'usp_clmu' object created. The current working directory will be bonded to CLMU-App. The subsequent step is to configure and run the model. The simulation parameters should then be configured and the model run by calling 'usp.run()'. For example, the case name, surface data input, atmospheric data input, the simulation start date, the stop option, etc should be set for the specific simulation. Notably, the simulation start date and simulation time range (start date: start date + a duration (STOP_N) of STOP_OPTION). Once the execution has been completed, the function will return a list of the result file locations. Users can refer to

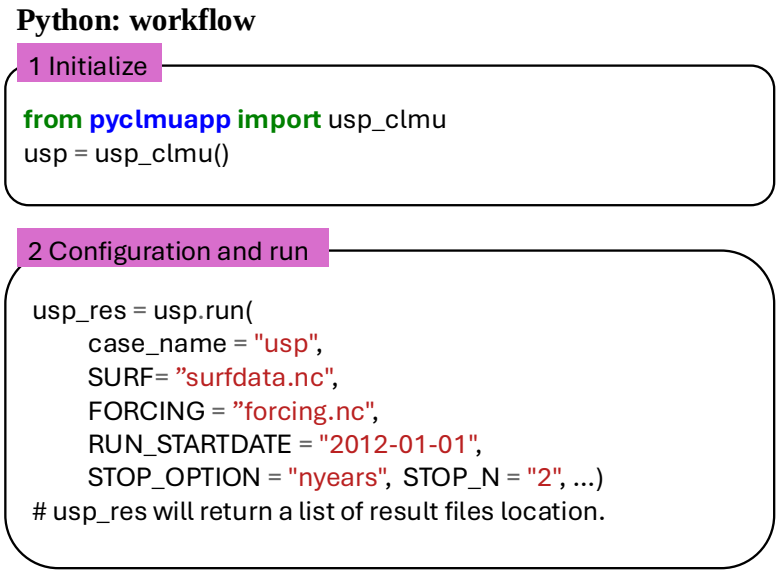

Fig. 4 Workflow of running CLMU simulations using Python.

Pyclmuapp document (https://envdes.github.io/pyclmuapp/) for the details of package details and instructions on installation, running simulation, and creating urban surface data and forcing data input.

4.2 Creating urban surface data

CLM also offers a variety of tools for creating user-customized single-point simulations. However, using these tools can be challenging because it requires compiling the programs, which necessitates complex environment configuration and even modification of some source code. Additionally, creating a single-point surface file often requires extensive input data, including source data on urban, soil, lakes, glaciers, etc. Here, Pyclmuapp focuses on urban environments, where the primary inputs are urban surface parameters and soil texture (K. Oleson et al., 2010).

To facilitate the creation of a user-customized urban surface input file, we provide a template file and users can replace the corresponding default parameters in the file using alternative user-specified urban surface data and soil texture data. When running the user-defined single-point simulation, we follow the minor modification of the newer version of CLMU to accommodate the updated urban surface data, in which ten layers (Nlevurb = 10) are now used for roofs and walls (K.W. Oleson & Feddema, 2020). This adjustment also strikes a balance between heat transfer modeling and computational efficiency (K.W. Oleson & Feddema, 2020).

The single-point land surface input data is extracted from urban surface data (https://svn-ccsm-inputdata.cgd.ucar.edu/trunk/inputdata/lnd/clm2/rawdata/mksrf_urban_0.05x0.05_simyr2000.c170724.nc) and soil texture data (https://svn-ccsm-inputdata.cgd.ucar.edu/trunk/inputdata/lnd/clm2/rawdata/mksrf_soitex.10level.c010119.nc). By providing the latitude and longitude for the point

of interest, the function will generate a 'surfdata.nc' (surface data for user-defined single-point simulation). The PTC_URBAN parameter in surface data represents the percentage of urban density types for the point of interest. Usually, the summary of PTC_URBAN should be 100 unless the parameters of other landunits are available. Otherwise, the other landunits of CLM may be active and the output will include other modules, e.g., vegetation and bare soil. In other words, the Pyclmuapp can simulate other landunits when the corresponding landunits parameters are available. For fully single point surface data applicable to other landunits, please refer to the CLM technical note (https://escomp.github.io/ctsm-docs/versions/release-clm5.0/html/).

The urban landunits include three classes (urban density types), namely tall building district (TBD), high density (HD), and medium density (MD) (Jackson et al., 2010; Lawrence et al., 2019). TBD urban is an area with buildings greater than or equal to ten stories tall, with a small pervious fraction (K.W. Oleson & Feddema, 2020). HD urban encompasses regions with buildings ranging from 3 to 10 stories tall and a pervious fraction between 5% and 25%, e.g., commercial, residential, or industrial areas. MD urban areas comprise row houses or apartment complexes 1 to 3 stories tall, with a pervious fraction ranging from 20% to 60% (K.W. Oleson & Feddema, 2020). Originally, the urban extent was derived from LandScan 2004, a population density dataset derived from census data, nighttime lights satellite observations, road proximity, and slope (K. Oleson et al., 2010). The details of urban surface data are described in K.W. Oleson and Feddema (2020). As most grid cells in the global urban data surface dataset are MD urban, the PCT_URBAN was set to '0,0,100' by default, meaning utilizing the full MD urban as surface input data. This method simplifies the configuration and modification process, enabling users to more easily create custom urban surface files that meet the new standards. The user can also modify the surface data ('surfdata.nc') to get different climate responses.

4.3 Creating atmospheric forcing data

The atmospheric forcing data for CLMU include the height of observational variables (Zbot; Unit: m), precipitation rate (Prectmms; Unit: mm/s), downward shortwave radiation (SWdown; Unit: W/m^2), downward longwave radiation (LWdown; Unit: W/m^2), wind speed at forcing height (Wind; Unit: m/s), surface pressure at forcing height (Psurf; Unit: pa), air temperature at forcing height (Tair; Unit: K), and specific air humidity at forcing height (Qair; Unit: kg/kg). The atmospheric forcing data can be sourced from both observational datasets and model simulations.

As observational data is not always available, we provide a feasible way to create atmospheric forcing from the fifth generation European Centre for Medium-Range Weather Forecasts reanalysis for the global climate and weather (ERA5) data. The package provides a tutorial and function to make the single-point forcing from ERA5 single levels hourly data. CLMU set a default forcing height of 30 meters. To standardize this height, the function provided by Pyclmuapp sets the default forcing height to 30 meters, and then the wind speed, air temperature, specific humidity, and pressure of ERA5 data will be adjusted according to the selected forcing height. The wind speed is then adjusted using the 'forecast surface roughness' variable, following the

method specified in (M.J. Lipson et al., 2024). The dew point temperature is converted to absolute humidity according to the same conversion formula used by CLM. The details of the calculation are in Section B. The forcing data is aggregated (on the dimension of time) into one file for the convenience of management.

4.4 Evaluation of Pyclmuapp performance

The Pyclmuapp-enabled simulations were evaluated using the observational atmospheric forcing data of Kings College, London, United Kingdom (UK-Kin) site from the Urban-Plumber Phase 2 project (https://urban-plumber.github.io/UK-KingsCollege/). The site is located in the Central Activities Zone (CAZ) of London, UK, which has a temperate marine climate (Kotthaus & Grimmond, 2014). It is classified as high-density UZE (Urban Zone for Energy partitioning) and compact midrise LCZ (Local Climate Zone) (Kotthaus & Grimmond, 2014). More details about the site are described in (Kotthaus & Grimmond, 2014; M. Lipson et al., 2022). The simulation follows the requirements of the Urban Plumber project, with a 12-year-long simulation – 10 years for the model spinup phase and 2 years for the analysis phase. Then, the simulation results were compared with the observations of the site.

The first simulation was operated using the default parameters created by Pyclmuapp. The results show that the mean absolute errors (MAE) for upward shortwave radiation (SWup), upward long-wave radiation (LWup), latent heat flux (Qle), sensible heat flux (Qh), and momentum flux (Qtau) are 4.69 W/m^2, 5.50 W/m^2, 23.39 W/m^2, 52.93 W/m^2, and 0.16 N/m^2, respectively (Fig. A1–A5). The scatter plot indicates that CLMU performs best for SWup and LWup, while the performance for Qle is relatively poor (Fig. A4). The diurnal distributions of the simulations and observations show that the default parameters result in an overestimation of Qle, but an underestimation of Qh and Qtau. In the next simulation, the parameters of CANYON_HWR, HT_ROOF, WTLUNIT_ROOF, and WTROAD_PERV were adjusted according to the site detail (Table 3). CLMU does not include vegetation within the urban canyon, so vegetation and water body areas are not accounted for. WTLUNIT_ROOF and WTROAD_PERV are calculated based on the areas of impervious surfaces and green areas (assumed to be permeable surfaces). After modifying these parameters, the simulation results for Qle and Qh improved, especially the distribution of Qle (Fig. A6–A10). This demonstrates that more realistic urban parameters can effectively enhance the performance of CLMU.

Table 3 Difference of urban surface parameters between different default case and detail case.

Variables	Default	Detail
CANYON_HWR	0.75	1.13
HT_ROOF	15	21.3
WTLUNIT_ROOF	0.35	0.47
WTROAD_PERV	0.68	0.15

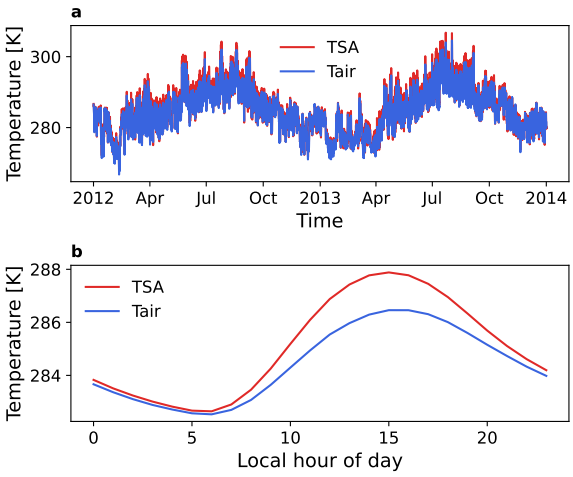

Fig. 5 Urban air temperatures from Pyclmuapp. **a** urban temperature and atmosphere temperature of 30 min time-step, **b** diurnal profile. TSA: 2m air temperature (the MD urban is 100%, so TSA is the MD urban 2m air temperature); Tair: the atmosphere temperature at observational height.

5 Case Studies

The use case configuration in the following is based on Section 4.4, where the forcing data is sourced from the UK-Kin site (same as Section 4.4), and the surface data is created using Pylcmuapp. The cases used the spin-up files derived from a ten-year simulation (2002/01/01-–2011/12/31), driven by UK-Kin site forcing and Pylcmuapp-generated surface data. Subsequently, three 2-year simulations were conducted: a) Use case (a) used the default UK-Kin forcing and surface data; b) Use case (b) employed modified forcing data. c) Use case (c) incorporated both modified forcing and surface data. The analysis period for these simulations spanned from 2012 to 2014.

5.1 Use case (a): Urban climate simulations

5.1.1 Urban temperatures

The CLMU simulations driven by atmospheric forcing can output urban air temperatures, which are different from the forcing temperatures. This process describes the impact of urban surfaces and anthropogenic emissions on urban climate. The results indicate that urbanization leads to an increase in air temperature, especially during the daytime (Fig. 5). During the daytime, urban cover absorbs and stores solar energy, causing surface temperatures to rise.

5.1.2 Radiation balance

Further analysis of energy balance can provide insights into climate and weather phenomena. The radiation balance can be described as equation 1,

$$Q* = \mathrm{SWdown} + \mathrm{LWdown} - \mathrm{SWup} - \mathrm{LWup}, \tag{1}$$

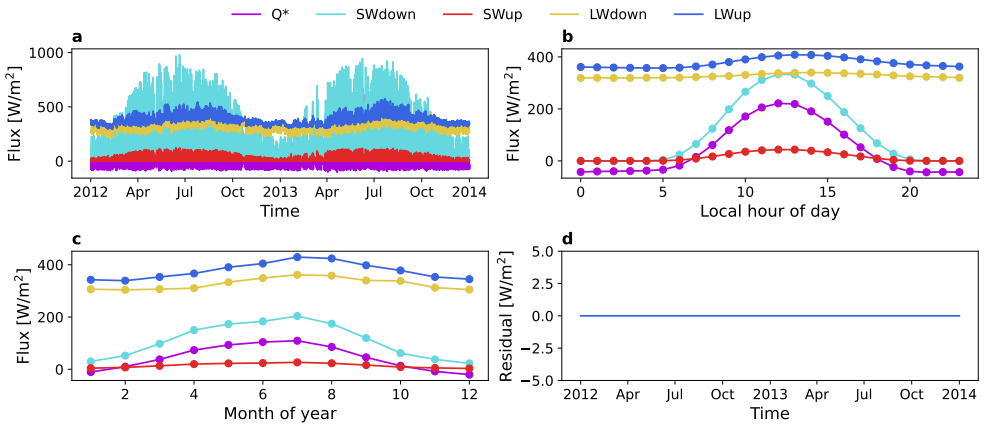

Fig. 6 Radiation flux balance. **a** 30 min time-step, **b** diurnal profile. **c** monthly profile, **d** residual of radiation balance. Q*: absorbed radiative energy flux, SWdown and LWdown: the downward solar radiation and longwave radiation from atmosphere forcing, SWup and LWup: upward solar radiation and longwave radiation. Residual is the difference of the left part and right part of equation 1

where Q* (W/m^2) is the surface net radiative energy flux; SWdown (W/m^2) and LWdown (W/m^2) are the downward solar radiation and longwave radiation from atmosphere forcing, respectively; and the SWup (W/m^2) and LWup (W/m^2) are the upward solar radiation and longwave radiation from land to the atmosphere, respectively.

The majority of allwave radiation is re-emitted to the atmosphere as longwave radiation, with a smaller fraction being reflected as shortwave radiation (Fig. 6). During the daytime, urban areas absorb a portion of this radiation while also reflecting some back into the atmosphere. At noon, when shortwave radiation reaches its peak, the amount of radiation absorbed by urban areas also reaches its maximum. As the incoming radiation decreases, the absorbed energy gradually diminishes and is subsequently released into the atmosphere as longwave radiation.

5.1.3 Surface energy balance

Urban energy balance can be expressed by equation 2,

$$Q* + Qanth = Qle + Qh + Qstor, \tag{2}$$

where Q* (W/m^2) is the storage radiative energy flux, Qanth, Qle, Qh and Qstor (W/m^2) are the anthropogenic heat flux, latent heat flux, sensible heat flux, and the storage heat flux, respectively. Qanth is the sum of waste heat from space heating and air conditioning, and the energy from space heating, and Qstor is the sum of heat flux into soil/snow, urban heating flux, and the heat flux from urban air conditioning (negative direction).

Most of the Q* is converted into Qstor in the morning (Fig. 7). The Qstor reaches its peak around noon, while sensible and latent heat continues to rise. At night, the Qstor is released and becomes negative, and latent heat begins to exceed sensible heat. Seasonal analysis indicates that in winter, the anthropogenic heat emissions increase,

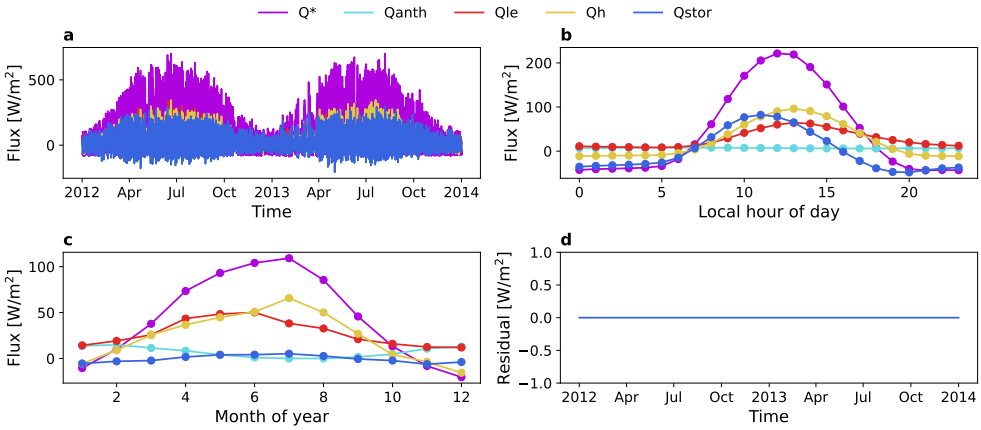

Fig. 7 Energy flux balance. **a** 30 min time-step, **b** diurnal profile. **c** monthly profile, **d** residual of energy balance. Q*: absorbed radiative energy flux, Qanth: anthropogenic heat flux, Qle: latent heat flux, Qh: sensible heat flux, Qstor: storage heat flux. Residual is the difference between the left part and right part of equation 2.

and the Qstor becomes negative. In summer, the Q* increases, and sensible heat rises markedly.

5.1.4 Variables of each canyon column

As previously mentioned, CLMU models the urban environment as a canyon, incorporating roofs, walls (both shaded and sunlit), and both impervious and pervious roads. Understanding the status of each surface is crucial for comprehending urban climate. Simulation results indicate that roofs generally exhibit the highest daytime skin temperatures, followed by sunlit walls and impervious roads, while pervious roads and shaded walls have the lowest temperatures (Fig. 8). Analysis of energy characteristics reveals that sunlit walls and roofs experience fewer variations in ground heat flux. The diurnal variation in the sensible heat of roofs is pronounced, mirroring the observed trends in roof skin temperatures, whereas the sensible heat flux of pervious roads is comparatively lower. The latent heat flux of pervious roads is more than that of roofs and impervious roads, and the latent heat flux of both sunlit walls and shaded walls is zero. This observed trend in latent heat is attributed to the fact that walls in LCMU are hydrologically inactive (i.e., precipitation is assumed to be vertical and hence doesn't impinge on walls). Given the typical dry state of the built surfaces, roofs and impervious roads exhibit relatively lower latent heat compared to pervious roads that account for most of the latent heat flux. These results imply that increasing the fraction of roofs and impervious roads will likely raise urban skin temperatures, whereas incorporating more pervious roads may reduce temperatures but could potentially increase latent heat flux.

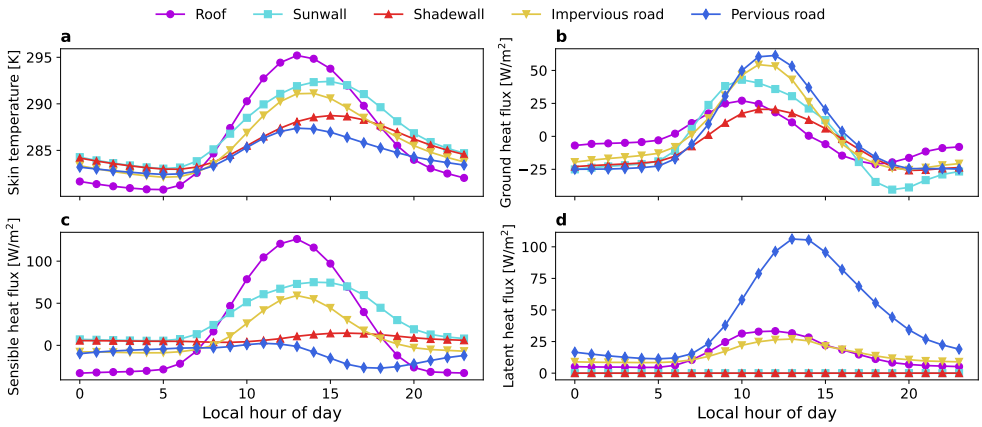

Fig. 8 Diurnal profiles of variables of each canyon column. **a** skin temperature, **b** ground heat flux, **c** sensible heat flux, **d** latent heat flux.

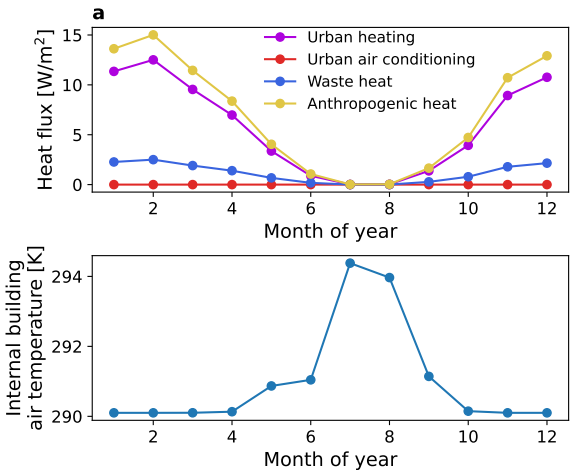

Fig. 9 Monthly profile of building energy flux (**a**) and internal building air temperature (**b**).

5.1.5 Building energy

In CLMU, the energy used to maintain indoor temperature is determined by air conditioning and building heating (K.W. Oleson & Feddema, 2020). The indoor air temperature variation shows that to maintain indoor temperatures, the heating system is activated during winter and early spring, leading to increased anthropogenic heat emissions (Fig. 9). During the summer, indoor temperatures do not reach the temperature threshold of turning on air conditioning defined by CLMU. Consequently, this simulation on this particular site does not include heat emissions from air conditioning.

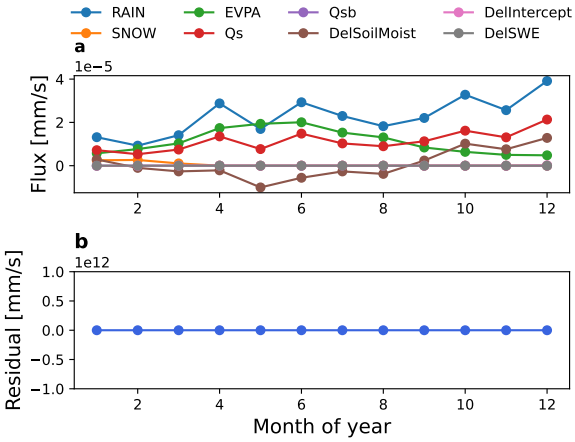

Fig. 10 Water balance of CLMU. **a** monthly profile of water flux. **b** residual of water balance. Residual is the difference between the left part and right part of equation 3

5.1.6 Water balance

The effects of urbanization on heat can further affect water allocation, e.g., increased evaporation can lead to more arid urban areas. For instance, an increase in impervious surfaces of cities leads to greater urban runoff (US EPA, 2020), and urban runoff is higher in high-density cities than in low-density cities (Gray et al., 2023). These connections illustrate that proper urban planning will play an important role in urban water stewardship. The hydrological result from urban climate modeling can model the influence of urbanization on urban water balance and be used as the input for other models to test onward impacts. CLMU incorporates hydrological processes from CLM, where the water balance equation can be presented as equation 3.

$$\mathrm{RAIN} + \mathrm{SNOW} = \mathrm{EVPA} + \mathrm{Qs} + \mathrm{Qsb} + \mathrm{DelSWE} + \mathrm{DelSoilMoist} + \mathrm{DelIntercept}, \tag{3}$$

where RAIN and SNOW are the rain and snow from the atmosphere; EVPA is the total evaporation including the canopy transpiration, canopy evaporation, and ground evaporation; Qs is the total runoff; Qsb is the subsurface drainage; DelSWE is the difference of snow depth (liquid water) divided by time-step; DelSoilMoist is the difference in soil moisture divided by time-step and weighted by pervious road column; DelIntercept is the difference in intercept water of roof and pervious road divided by time-step. The simulation results indicate that urban water storage increases during seasons with higher rainfall (autumn and winter), along with an increase in runoff, while evaporation remains relatively low. In spring, water storage decreases sharply, and evaporation reaches its peak, which could potentially lead to dry conditions. In May, rainfall and soil moisture decreased, but evaporation remained high (Fig. 10).

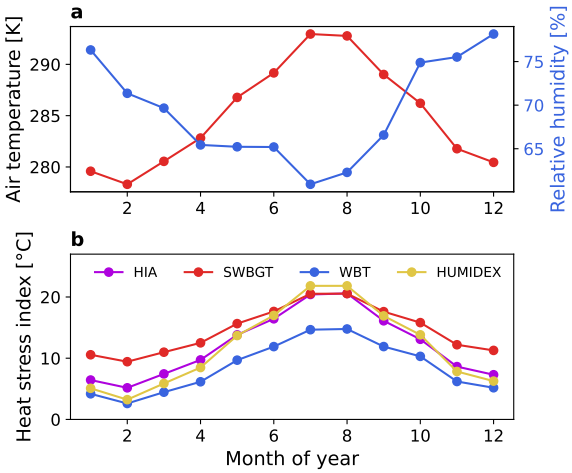

Fig. 11 Monthly profile of air temperature and humidity (**a**) and heat stress indices (**b**). HIA represents the 2m NWS heat index, SWBGT represents the 2m simplified wet-bulb globe temperature, and WBT represents the 2m wet-bulb temperature

5.1.7 Heat stress index

Cities are the primary areas where humans reside. For humans, temperature differences are not the only factor affecting heat dissipation. The heat stress index combines atmospheric temperature, humidity and wind, taking sweat evaporation into account. CLMU can output urban temperature and humidity, which can be used to calculate various heat stress factors. Additionally, CLM has implemented the calculation of multiple heat stress indices, enabling output through the HumanIndexMod module (Buzan, Oleson, & Huber, 2015). The results of heat stress indices show that in summer, the temperature is highest, humidity is lowest, and heat stress indices are at their peak (Fig. 10).

5.2 Use case (b): Global warming

Climate change is significantly affecting urban climate. Pyclmuapp provides a function that allows for the rapid modification of forcing variables to explore the potential impacts of future climate change on urban climate. With this functionality, stakeholders can make informed decisions while considering various warming scenarios. In this example, we analyzed the impact of an increase of 1 Kelvin degree (1 K) in atmospheric temperature on urban air temperature. With only the atmospheric temperature increasing, the result shows an increasing trend but no significant changes in its diurnal distribution (Fig. 12). However, the impact of increased atmospheric temperature on urban air temperature varies over time. In most cases, the increase in urban temperature is less than the increase in atmospheric temperature (1 K). At certain times, the change in urban temperature exceeds 1 K.

The overall future climate warming has the greatest impact during the daytime (Fig. 12). This information is valuable. For example, simple measures, like white roofs,

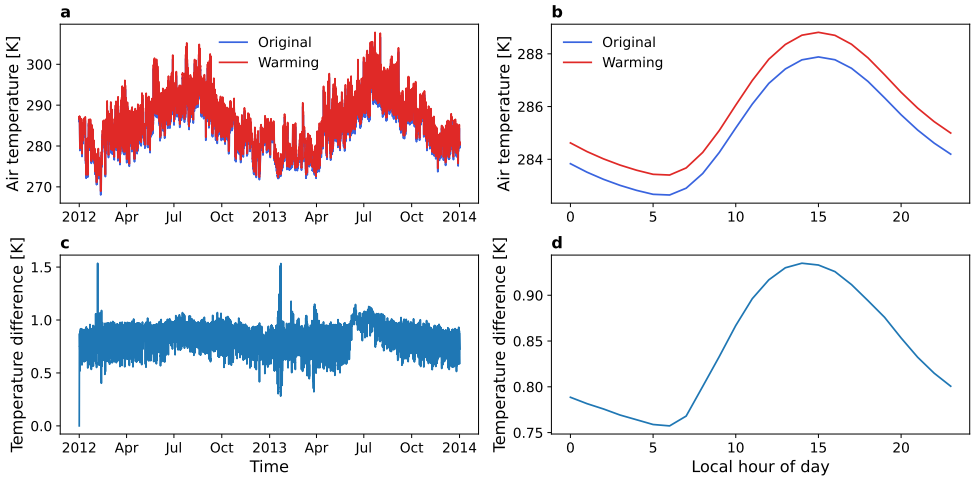

Fig. 12 Variation in urban air temperature of different scenarios. **a** 30 min time-step, **b** diurnal profile. **c** 30 min time-step and **d** diurnal profiles of difference in urban air temperature between the original forcing and a warming scenario. The warming scenario is represented by an increase in atmosphere temperature by 1K.

can directly reflect solar radiation, thereby reducing daytime urban temperatures. In the context of rising atmospheric temperatures, the benefits of such measures might be greater since the impact of increased atmospheric temperature on daytime urban temperatures is higher.

5.3 Use case (c): Urban climate adaptation

The CLMU parameterization of urban columns includes roofs, walls, impervious roads, and pervious roads. Each column has its characteristics, e.g., emissivity, albedo, and heat capacity (K. Oleson et al., 2010). These parameters digitally represent the urban environment, allowing for the simulation of different urban development scenarios and adaptation strategies to assess their impact on climate. For instance, by modifying parameters like canyon height-to-width ratio and roof height, one can simulate the impact of future urban development on climate.

Roof modifications are relatively straightforward and feasible, and are a common measure in urban climate adaptation studies (Georgescu, Broadbent, & Krayenhoff, 2024; L. Wang et al., 2020; Z.-H. Wang, 2021). In this example, the albedo of roofs (both direct and diffuse albedo) was modified to simulate the implementation of cool roofs and their impact on climate (Sun et al., 2024). The results indicate that increasing roof albedo effectively reduces urban air temperatures, with the reduction being most pronounced during the daytime (Fig. 13). As future temperatures rise, the effectiveness of cool roofs increases, making both daytime and nighttime benefits more.

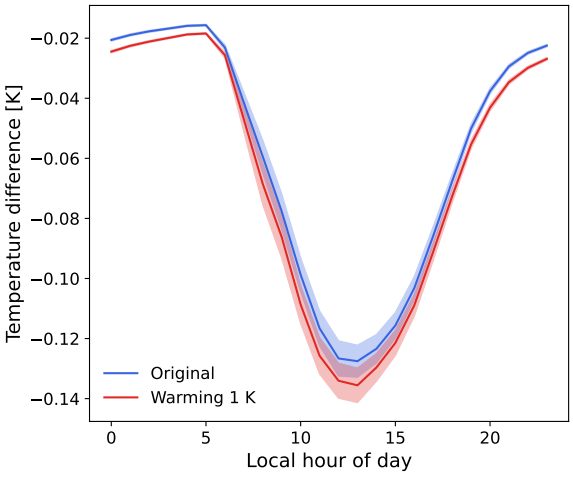

Fig. 13 Variation in hourly urban air temperature of different scenarios. Original: increasing roof direct reflection albedo by 0.2. Warming: increasing 1 K of Tair of atmospheric forcing with increasing roof albedo by 0.2.

6 Implication, Limitation and Future Work

Vast investments are being made in urban climate adaptation actions (Diezmartínez & Short Gianotti, 2024). The Sixth Assessment Report (AR6) of the United Nations (UN) Intergovernmental Panel on Climate Change (IPCC) underscores a disconnection between urban adaptation investment and the evolution of policy and practice innovations, with numerous cities conceptualizing climate adaptation blueprints yet few transitioning to implementation (Dodman et al., 2022). The diffusion of adaptation strategies mandates consideration not only of climatic effects but also of financial outlay, administrative capabilities, and related factors. Therefore, it is crucial to formulate plans that balance cost and climate considerations. With advancements in urban climate models, urban planning using these models has become more feasible. However, a significant entry barrier remains in the effective use of these models. This study provides a toolkit for streamlining urban climate simulations, enabling scientists and stakeholders from various disciplines to leverage advanced urban climate models. By analyzing the impact of urban parameters on climate, the toolkit allows for the assessment of different scenarios, facilitating the integration of climate factors into traditional urban planning. Compared to traditional modeling approaches that rely on pre-defined climate variables derived from scenario outcomes, this toolkit offers several advantages: (1) the open-source nature democratizes access, making it feasible for smaller municipalities, non-governmental organizations, and academic institutions, (3) the customization of simulations according to specific urban parameters and climate goals, and (4) the efficient exploration of adaptation strategies. For example, using this toolkit as a data generator and integrating the optimization algorithms, the potentially suitable configuration of building materials or urban morphology can be obtained. This approach accelerates the search for effective solutions, reducing the

need for manual tuning and trial-and-error, while ensuring that the final strategy is both feasible and effective under projected climate conditions.

It is important to note that CLMU is primarily designed for mesoscale/large-scale climate modeling. Therefore, in local or micro-scale simulations, using the micro-scale models or computational fluid dynamic models will be more useful. However, CLMU can still provide advantages due to the limited computational cost of single-point modeling, because there is a huge computational cost for running micro-scale models and computational fluid dynamic models. A hybrid approach that leverages the strengths of both CLMU and micro-scale models could be advantageous. CLMU could provide the background climate input for detailed simulations using micro-scale models.

In the future, posting Pyclmuapp/CLMU-App into a cloud-based platform is a promising solution. These strategies also help users easily get access to the more forcing data and avoid downloading and installing Pyclmuapp, making it a real out-of-the-box toolkit. Thus, this application will help decision-making in urban climate-related problems (e.g., urban climate adaptation planning, urban health, etc.) and education.

7 Conclusions

By being fully open-source, CLMU enables a broader audience to benefit from advanced urban climate modeling. However, conducting a CLMU simulation still faces challenges due to the complexities of model installation, environment and case configuration, and generation of the model inputs. This study uses the container technique to build up a container application (CLMU-App) to enable the operating system-independent simulation and avoid the complexities in installation and environment configuration. A Python package (Pyclmuapp) is further developed to streamline the execution of the containerized CLMU and the creation of input data. Using Pyclmuapp, users can: (1) simulate urban climate changes, analyze their causes, explore potential urban human emissions and energy consumption, and analyze urban water balance and human thermal stress; (2) simulate the impact of future climate change on urban climate by altering forcing variables. (3) explore the response of urban climate to different urban surface properties by modifying urban surface parameters.

Acknowledgements. This work used the ARCHER2 UK National Supercomputing Service (https://www.archer2.ac.uk). The authors would like to acknowledge the assistance given by Research IT and the use of the HPC Pool and Computational Shared Facility at The University of Manchester. Z.Z. appreciates the support provided by the academic start-up funds from the Department of Earth and Environmental Sciences at The University of Manchester. J.Y. acknowledges support from the China Scholarship Council. Contributions from K.W.O. are based upon work supported by the NSF National Center for Atmospheric Research, which is a major facility sponsored by the U.S. National Science Foundation under Cooperative Agreement No. 1852977.

Appendix A Validation results of Pyclmuapp

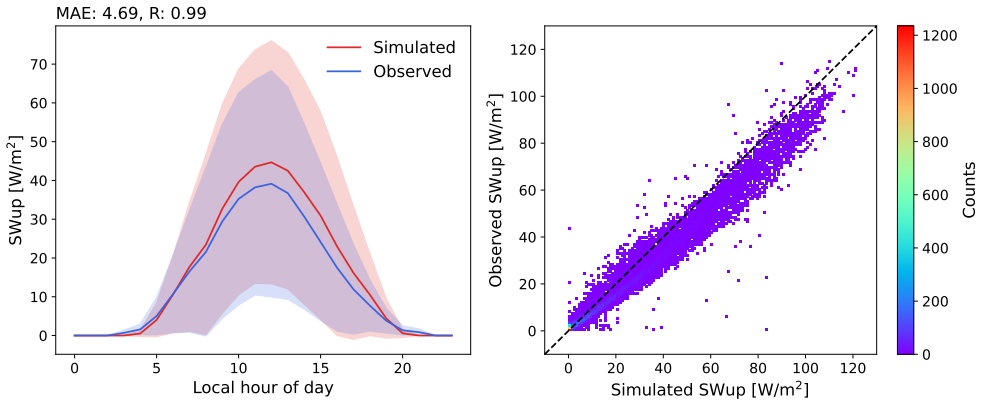

Fig. A1 Short wave radiation flux (upward) Evaluation of Pyclmuapp default parameters for UK-Kin site. Spinup period: 2002-2012; Analysis period: 2012-2014.

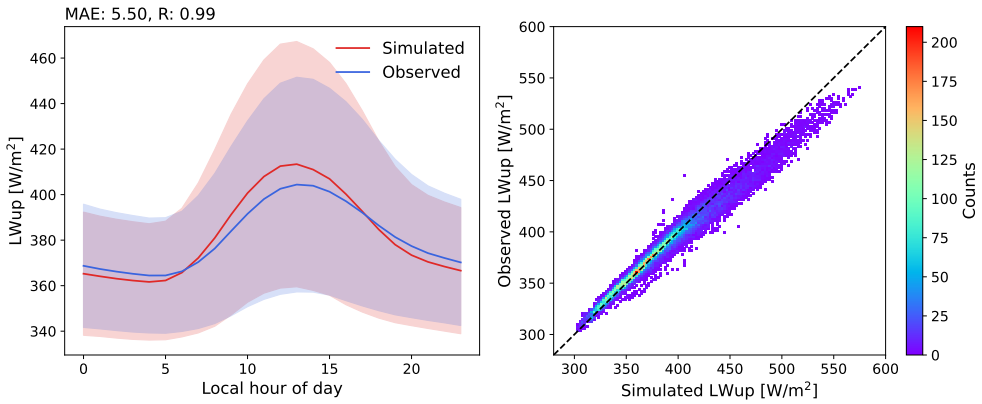

Fig. A2 Long wave radiation flux (upward) evaluation of Pyclmuapp default parameters for UK-Kin site. Spinup period: 2002-2012; Analysis period: 2012-2014.

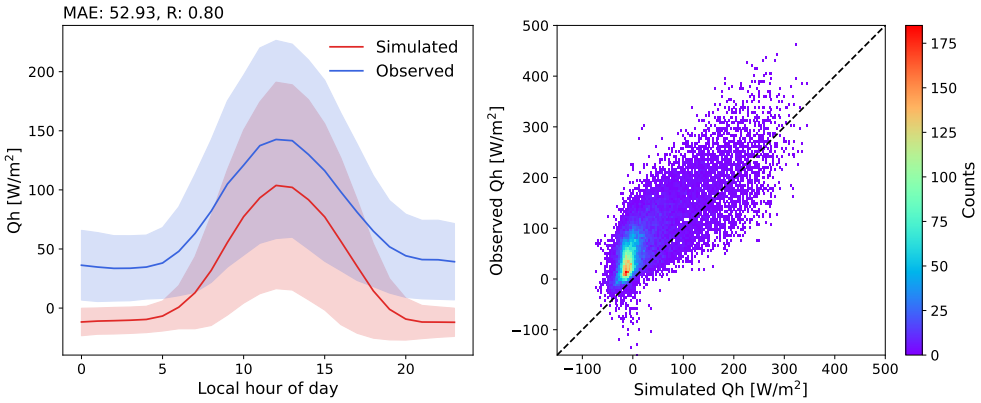

Fig. A3 Sensible heat flux evaluation of Pyclmuapp default parameters for UK-Kin site. Spinup period: 2002-2012; Analysis period: 2012-2014.

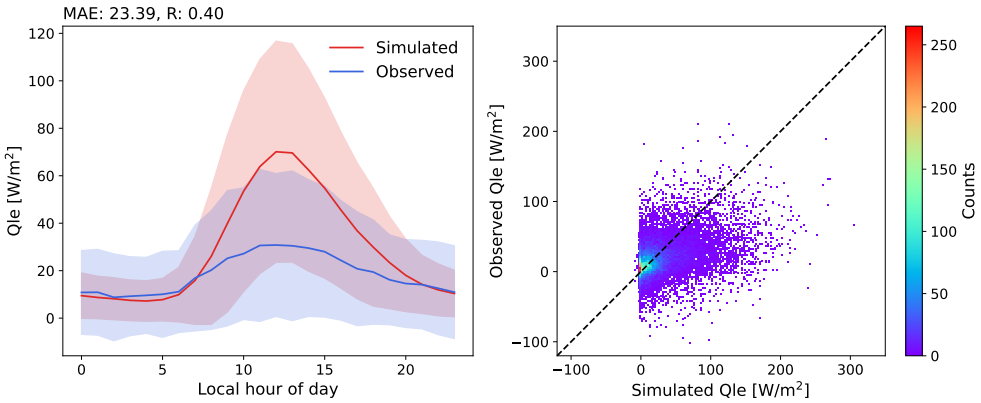

Fig. A4 Latent heat flux evaluation of Pyclmuapp default parameters for UK-Kin site. Spinup period: 2002-2012; Analysis period: 2012-2014.

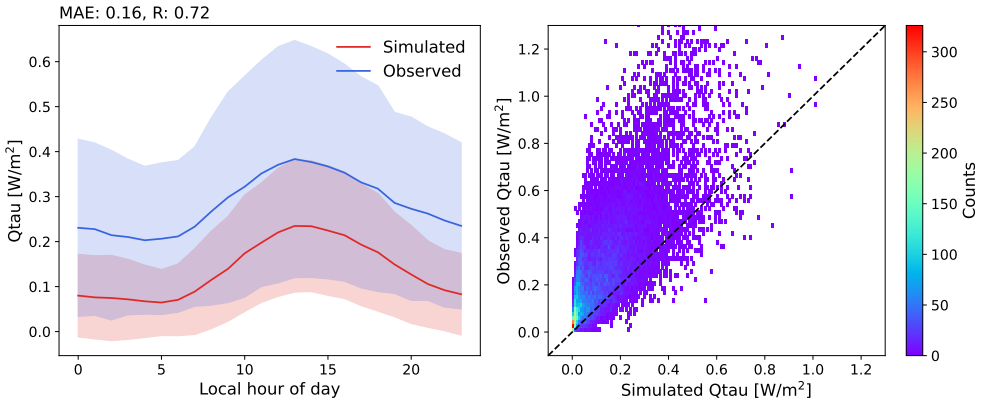

Fig. A5 Momentum flux evaluation of Pyclmuapp default parameters for UK-Kin site. Spinup period: 2002-2012; Analysis period: 2012-2014.

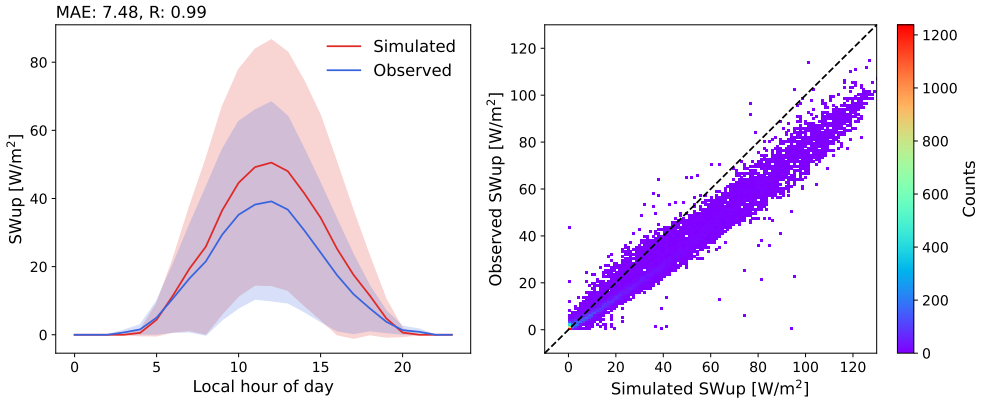

Fig. A6 Short wave radiation flux (upward) Evaluation of Pyclmuapp with CANYON_HWR, HT_ROOF, WTLUNIT_ROOF, WTROAD_PERV and soil texture adjusted for UK-Kin site. Spinup period: 2002-2012; Analysis period: 2012-2014.

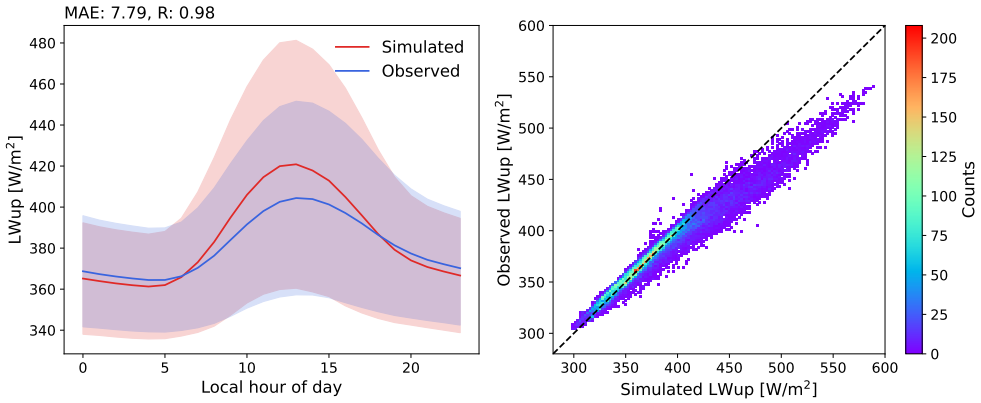

Fig. A7 Long wave radiation flux (upward) evaluation of Pyclmuapp with CANYON_HWR, HT_ROOF, WTLUNIT_ROOF, WTROAD_PERV and soil texture adjusted for UK-Kin site. Spinup period: 2002-2012; Analysis period: 2012-2014.

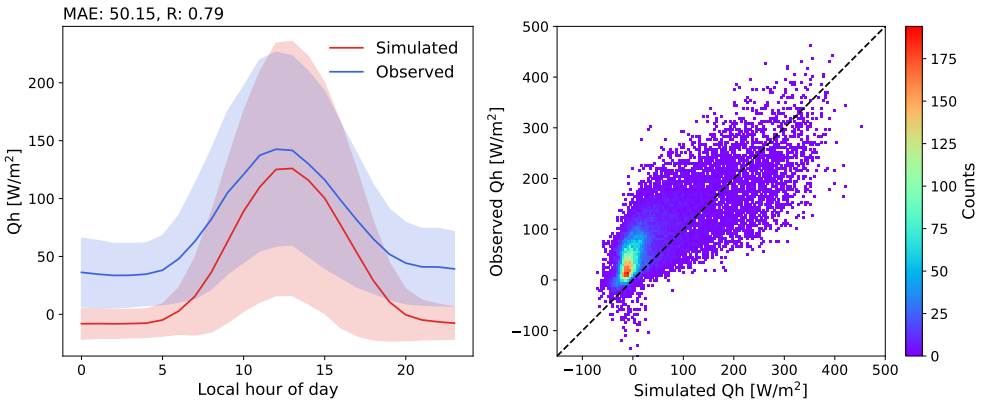

Fig. A8 Sensible heat flux evaluation of Pyclmuapp with CANYON_HWR, HT_ROOF, WTLUNIT_ROOF, WTROAD_PERV and soil texture adjusted for UK-Kin site. Spinup period: 2002-2012; Analysis period: 2012-2014.

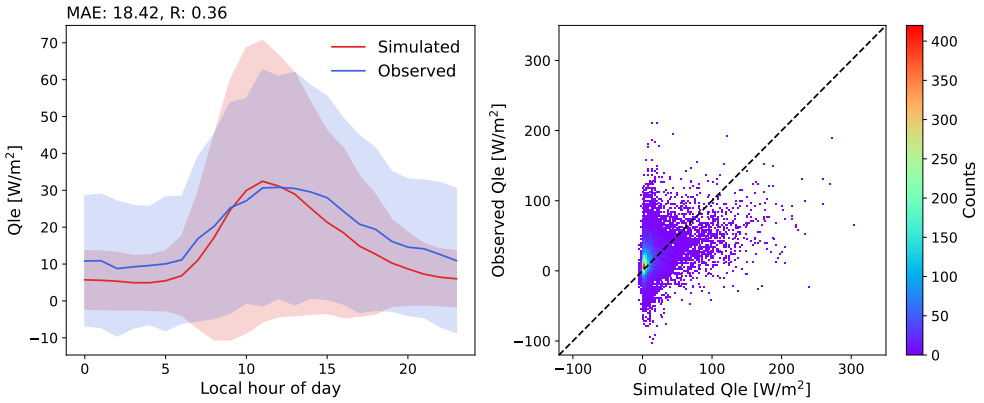

Fig. A9 Latent heat flux evaluation of Pyclmuapp with CANYON_HWR, HT_ROOF, WTLUNIT_ROOF, WTROAD_PERV and soil texture adjusted for UK-Kin site. Spinup period: 2002-2012; Analysis period: 2012-2014.

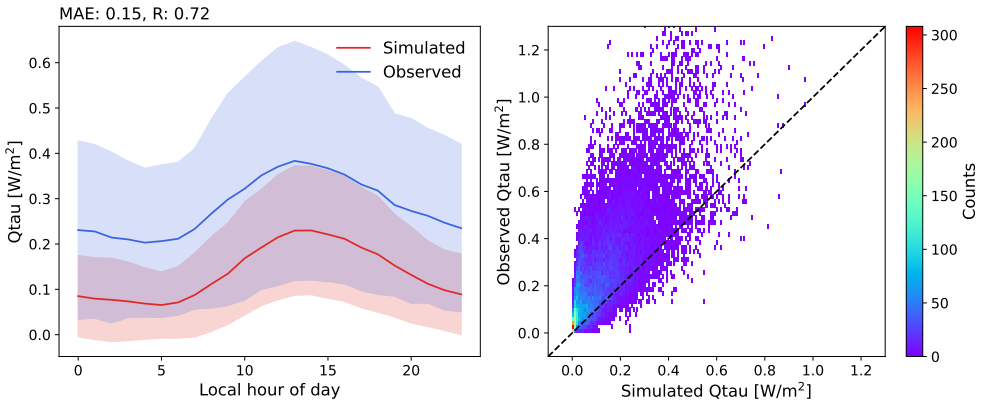

Fig. A10 Momentum flux evaluation of Pyclmuapp with CANYON_HWR, HT_ROOF, WTLUNIT_ROOF, WTROAD_PERV and soil texture adjusted for UK-Kin site. Spinup period: 2002-2012; Analysis period: 2012-2014.

Appendix B Forcing calculation from ERA5 data

B.1 Air temperature

$$T_{z1} = T_{z0} - R_{lapse} * (z1 - z0), \tag{B1}$$

where $z1$ and $z0$ are the heights (m), respectively; T_{z1} and T_{z0} (K) are the air temperature at $z1$ and $z0$, respectively; R_{lapse} is the lapse rate (K/m), default is 0.006 for simplicity, according to CTSM.

B.2 Pressure

$$P_{z1} = P_{z0} * exp(-(z1 - z0)/H), \tag{B2}$$

$$H = 0.5 * r_{air} * (T_{z1} + T_{z0})/g, \tag{B3}$$

$$r_{air} = k * N_A/M, \tag{B4}$$

where $z1$ and $z0$ are the heights (m), respectively; P_{z1} and P_{z0} (Pa) are the pressure at $z1$ and $z0$, respectively; T_{z1} and T_{z0} (K) are the air temperature at $z1$ and $z0$, respectively; r_{air} is the dry air gas constant (J/(K·kg); g acceleration of gravity (m/s^2). k is the Boltzmann's constant (J/(K·molecule)), default is 1.38065*10^{-23}; N_A is the Avogadro's number (molecules/kmole), default is 6.02214*10^{26}; M is the molecular weight dry air (kg/kmole), default is 28.966.

B.3 Wind

$$w = (u^2 + v^2)^(0.5) \tag{B5}$$

$$w_{z1} = w_{z0} * \frac{ln(z1/fsr)}{ln(z0/fsr)} \tag{B6}$$

where w are the wind speed (m/s), u and v are the u-component of wind and v-component of wind (m/s), respectively; $z1$ and $z0$ are the heights (m), respectively; fsr is the forecast surface roughness (m).

B.4 Humidity

$$Q_{z1} = \frac{0.622 * es}{P_{z1} - 0.622 * es} \tag{B7}$$

where

$$es = 100*(a0+td_{z1}*(a1+td_{z1}*(a2+td_{z1}*(a3+td_{z1}*(a4+td_{z1}*(a5+td_{z1}*(a6+td_{z1}*(a7+td_{z1}*a8))))))))) \tag{B8}$$

$$td_{z1} = td_{z0} - R_{lapse} * (z1 - z0) \tag{B9}$$

where Q_{z1} is the specific humidity at $z1$ (kg/kg); P_{z1} is the pressure at $z1$ (pa); es is the vapor pressure (pa); $z1$ and $z0$ are the heights (m), respectively; Td is the dew point temperature (°C); the es is calculate by polynomial fit (Flatau, Walko, & Cotton, 1992), when $0 < Td <= 100$, a0–a8 are 6.11213476, 0.444007856, 0.143064234e-01, 0.264461437e-03, 0.305903558e-05, 0.196237241e-07, 0.892344772e-10, -0.373208410e-12, and 0.209339997e-15 respectively, when $-75 < Td <= 0$, a0–a8 are, 6.11123516, 0.503109514, 0.188369801e-01, 0.420547422e-03, 0.614396778e-05, 0.602780717e-07, 0.387940929e-09, 0.149436277e-11, and 0.262655803e-14 respectively. Reference code implementation is QSatMod.F90 of CTSM. This calculation assumes the water content is less affected by the slightly different heights of 30m and 2m.

References

Adilkhanova, I., Santamouris, M., Yun, G.Y. (2024). Green roofs save energy in cities and fight regional climate change. *Nature Cities*, *1*(3), 238–249, https://doi.org/10.1038/s44284-024-00035-7

Anderson, G.B., Oleson, K.W., Jones, B., Peng, R.D. (2018). Projected trends in high-mortality heatwaves under different scenarios of climate, population, and adaptation in 82 US communities. *Climatic Change*, *146*(3), 455–470, https://doi.org/10.1007/s10584-016-1779-x

Bao, Q., Liu, Y., Wu, G., He, B., Li, J., Wang, L., ... Zhang, X. (2020). CAS FGOALS-f3-H and CAS FGOALS-f3-L outputs for the high-resolution model intercomparison project simulation of CMIP6. *Atmospheric and Oceanic Science Letters*, *13*(6), 576–581, https://doi.org/10.1080/16742834.2020.1814675

Buzan, J.R., Oleson, K., Huber, M. (2015). Implementation and comparison of a suite of heat stress metrics within the Community Land Model version 4.5. *Geoscientific Model Development*, *8*(2), 151–170, https://doi.org/10.5194/gmd-8-151-2015

Demuzere, M., Harshan, S., Järvi, L., Roth, M., Grimmond, C.S.B., Masson, V., ... Wouters, H. (2017). Impact of urban canopy models and external parameters on the modelled urban energy balance in a tropical city. *Quarterly Journal of the Royal Meteorological Society*, *143*(704), 1581–1596, https://doi.org/10.1002/qj.3028

Diezmartínez, C.V., & Short Gianotti, A.G. (2024). Municipal finance shapes urban climate action and justice. *Nature Climate Change*, *14*(3), 247–252, https://doi.org/10.1038/s41558-024-01924-4

Dimoudi, A., Kantzioura, A., Zoras, S., Pallas, C., Kosmopoulos, P. (2013). Investigation of urban microclimate parameters in an urban center. *Energy and Buildings*, *64*, 1–9, https://doi.org/10.1016/j.enbuild.2013.04.014

Dodman, D., Hayward, B., Pelling, M., Broto, V.C., Chow, W., Chu, E., ... Ziervogel, G. (2022). Cities, settlements and key infrastructure. H.-O. Pörtner et al. (Eds.), *Climate Change 2022: Impacts, Adaptation and Vulnerability. Contribution of Working Group II to the Sixth Assessment Report of the Intergovernmental Panel on Climate Change* (pp. 907–1040). Cambridge, UK and New York, NY, USA: Cambridge University Press.

Fitria, R., Kim, D., Baik, J., Choi, M. (2019). Impact of Biophysical Mechanisms on Urban Heat Island Associated with Climate Variation and Urban Morphology. *Scientific Reports*, *9*(1), 19503, https://doi.org/10.1038/s41598-019-55847-8

Flatau, P.J., Walko, R.L., Cotton, W.R. (1992). Polynomial fits to saturation vapor

pressure. *Journal of Applied Meteorology and Climatology*, *31*(12), 1507–1513, https://doi.org/10.1175/1520-0450(1992)031⟨1507:PFTSVP⟩2.0.CO;2

Georgescu, M., Broadbent, A.M., Krayenhoff, E.S. (2024). Quantifying the decrease in heat exposure through adaptation and mitigation in twenty-first-century US cities. *Nature Cities*, *1*(1), 42–50, https://doi.org/10.1038/s44284-023-00001-9

Ghanbari, M., Arabi, M., Georgescu, M., Broadbent, A.M. (2023). The role of climate change and urban development on compound dry-hot extremes across US cities. *Nature Communications*, *14*(1), 3509, https://doi.org/10.1038/s41467-023-39205-x

Golaz, J.-C., Caldwell, P.M., Van Roekel, L.P., Petersen, M.R., Tang, Q., Wolfe, J.D., ... Zhu, Q. (2019). The DOE E3SM coupled model version 1: Overview and evaluation at standard resolution. *Journal of Advances in Modeling Earth Systems*, *11*(7), 2089–2129, https://doi.org/10.1029/2018MS001603

Gray, L.C., Zhao, L., Stillwell, A.S. (2023). Impacts of climate change on global total and urban runoff. *Journal of Hydrology*, *620*, 129352, https://doi.org/10.1016/j.jhydrol.2023.129352

Grimmond, C., Best, M., Barlow, J., Arnfield, A.J., Baik, J.-J., Baklanov, A., ... Williamson, T. (2009). Urban surface energy balance models: Model characteristics and methodology for a comparison study. A. Baklanov, G. Sue, M. Alexander, & M. Athanassiadou (Eds.), *Meteorological and air quality models for urban areas* (pp. 97–123). Berlin, Heidelberg: Springer Berlin Heidelberg.

Hu, J., He, G., Meng, R., Gong, W., Ren, Z., Shi, H., ... Ma, W. (2023). Temperature-related mortality in China from specific injury. *Nature Communications*, *14*(1), 37, https://doi.org/10.1038/s41467-022-35462-4

Jackson, T.L., Feddema, J.J., Oleson, K.W., Bonan, G.B., Bauer, J.T. (2010). Parameterization of Urban Characteristics for Global Climate Modeling. *Annals of the Association of American Geographers*, *100*(4), 848–865, https://doi.org/10.1080/00045608.2010.497328

Kotthaus, S., & Grimmond, C. (2014). Energy exchange in a dense urban environment – Part I: Temporal variability of long-term observations in central London. *Urban Climate*, *10*, 261–280, https://doi.org/10.1016/j.uclim.2013.10.002

Lawrence, D.M., Fisher, R.A., Koven, C.D., Oleson, K.W., Swenson, S.C., Bonan, G., ... Zeng, X. (2019). The community land model version 5: Description of new features, benchmarking, and impact of forcing uncertainty. *Journal of Advances in Modeling Earth Systems*, *11*(12), 4245–4287, https://doi.org/10.1029/2018MS001583

Li, C., & Zhang, N. (2021). Analysis of the daytime urban heat island mechanism in east china. *Journal of Geophysical Research: Atmospheres*, *126*(12), e2020JD034066, https://doi.org/10.1029/2020JD034066

Li, C., Zhang, N., Ren, K., Zhao, W., Wu, J., Sun, Y. (2024). Biophysical drivers of seasonal hysteresis of urban heat islands across climates and urban landscapes. *Journal of Geophysical Research: Atmospheres*, *129*(9), e2023JD040446, https://doi.org/10.1029/2023JD040446

Li, C., Zhang, N., Wang, Y., Chen, Y. (2023). Modeling urban heat islands and thermal comfort during a heat wave event in east china with CLM5 incorporating local climate zones. *Journal of Geophysical Research: Atmospheres*, *128*(16), e2023JD038883, https://doi.org/10.1029/2023JD038883

Li, D., Wang, L., Liao, W., Sun, T., Katul, G., Bou-Zeid, E., Maronga, B. (2024). Persistent urban heat. *Science Advances*, *10*(15), eadj7398, https://doi.org/10.1126/sciadv.adj7398

Lipson, M., Grimmond, S., Best, M., Chow, W.T.L., Christen, A., Chrysoulakis, N., ... Ward, H.C. (2022). Harmonized gap-filled datasets from 20 urban flux tower sites. *Earth System Science Data*, *14*(11), 5157–5178, https://doi.org/10.5194/essd-14-5157-2022

Lipson, M.J., Grimmond, S., Best, M., Abramowitz, G., Coutts, A., Tapper, N., ... Pitman, A.J. (2024). Evaluation of 30 urban land surface models in the Urban-PLUMBER project: Phase 1 results. *Quarterly Journal of the Royal Meteorological Society*, *150*(758), 126–169, https://doi.org/10.1002/qj.4589

Lovato, T., Peano, D., Butenschön, M., Materia, S., Iovino, D., Scoccimarro, E., ... Navarra, A. (2022). CMIP6 simulations with the CMCC earth system model (CMCC-ESM2). *Journal of Advances in Modeling Earth Systems*, *14*(3), e2021MS002814, https://doi.org/10.1029/2021MS002814

Lyu, H., Wang, W., Zhang, K., Cao, C., Xiao, W., Lee, X. (2024). Factors Influencing the Spatial Variability of Air Temperature Urban Heat Island Intensity in Chinese Cities. *Advances in Atmospheric Sciences*, *41*(5), 817–829, https://doi.org/10.1007/s00376-023-3012-y

Mohammad Harmay, N.S., & Choi, M. (2023). The urban heat island and thermal heat stress correlate with climate dynamics and energy budget variations in multiple urban environments. *Sustainable Cities and Society*, *91*, 104422, https://doi.org/10.1016/j.scs.2023.104422

Nilsen, I.B., Hanssen-Bauer, I., Dyrrdal, A.V., Hisdal, H., Lawrence, D., Haddeland, I., Wong, W.K. (2022). From climate model output to actionable climate information in norway. *Frontiers in Climate*, *4*, , https://doi.org/10.3389/fclim.2022.866563

Oke, T.R. (1987). *Boundary Layer Climates* (2nd ed.). Routledge.

Oke, T.R., Mills, G., Christen, A., Voogt, J.A. (2017a). Energy balance. *Urban climates* (pp. 156–196). Cambridge: Cambridge University Press.

Oke, T.R., Mills, G., Christen, A., Voogt, J.A. (2017b). Introduction. *Urban climates* (pp. 1–13). Cambridge: Cambridge University Press.

Oleson, K., Bonan, G., Feddema, J., Vertenstein, M., Kluzek, E. (2010). *Technical Description of an Urban Parameterization for the Community Land Model (CLMU)* (Tech. Rep.).

Oleson, K.W., & Feddema, J. (2020). Parameterization and surface data improvements and new capabilities for the community land model urban (CLMU). *Journal of Advances in Modeling Earth Systems*, *12*(2), e2018MS001586, https://doi.org/10.1029/2018MS001586

Potere, D., & Schneider, A. (2007). A critical look at representations of urban areas in global maps. *GeoJournal*, *69*(1), 55–80, https://doi.org/10.1007/s10708-007-9102-z

Ritchie, H., Samborska, V., Roser, M. (2024). Urbanization. *Our World in Data*, ,

Schneider, A., Friedl, M.A., Potere, D. (2009). A new map of global urban extent from MODIS satellite data. *Environmental Research Letters*, *4*(4), 044003, https://doi.org/10.1088/1748-9326/4/4/044003

Seland, Ø., Bentsen, M., Olivié, D., Toniazzo, T., Gjermundsen, A., Graff, L.S., ... Schulz, M. (2020). Overview of the norwegian earth system model (NorESM2) and key climate response of CMIP6 DECK, historical, and scenario simulations. *Geoscientific Model Development*, *13*(12), 6165–6200, https://doi.org/10.5194/gmd-13-6165-2020

Shahrestani, M., Yao, R., Luo, Z., Turkbeyler, E., Davies, H. (2015). A field study of urban microclimates in London. *Renewable Energy*, *73*, 3–9, https://doi.org/10.1016/j.renene.2014.05.061

Sun, Y., Fang, B., Oleson, K., Zhao, L., Topping, D., Schultz, D., Zheng, Z. (2024). *Improving Urban Climate Adaptation Modelling in the Community Earth System Model (CESM) Through Transient Urban Surface Albedo Representation.*

Urban Systems and Other Settlements. (2023). Intergovernmental Panel on Climate Change (IPCC) (Ed.), *Climate Change 2022 - Mitigation of Climate Change: Working Group III Contribution to the Sixth Assessment Report of the Intergovernmental Panel on Climate Change* (pp. 861–952). Cambridge: Cambridge University Press.

US EPA, OW. (2020). *Urbanization and Stormwater Runoff* [Overviews and Factsheets]. https://www.epa.gov/sourcewaterprotection/urbanization-and-stormwater-runoff.

Wang, J., Chen, Y., Liao, W., He, G., Tett, S.F.B., Yan, Z., ... Hu, Y. (2021). Anthropogenic emissions and urbanization increase risk of compound hot extremes in cities. *Nature Climate Change*, *11*(12), 1084–1089, https://doi.org/10.1038/s41558-021-01196-2

Wang, L., Huang, M., Li, D. (2020). Where are white roofs more effective in cooling the surface? *Geophysical Research Letters*, *47*(15), e2020GL087853, https://doi.org/10.1029/2020GL087853

Wang, L., Sun, T., Zhou, W., Liu, M., Li, D. (2023). Deciphering the sensitivity of urban canopy air temperature to anthropogenic heat flux with a forcing-feedback framework. *Environmental Research Letters*, *18*(9), 094005, https://doi.org/10.1088/1748-9326/ace7e0

Wang, Z.-H. (2021). Compound environmental impact of urban mitigation strategies: Co-benefits, trade-offs, and unintended consequence. *Sustainable Cities and Society*, *75*, 103284, https://doi.org/10.1016/j.scs.2021.103284

Yang, J., Zhao, L., Oleson, K. (2023). Large humidity effects on urban heat exposure and cooling challenges under climate change. *Environmental Research Letters*, *18*(4), 044024, https://doi.org/10.1088/1748-9326/acc475

Yin, J., Gentine, P., Slater, L., Gu, L., Pokhrel, Y., Hanasaki, N., ... Schlenker, W. (2023). Future socio-ecosystem productivity threatened by compound drought–heatwave events. *Nature Sustainability*, *6*(3), 259–272, https://doi.org/10.1038/s41893-022-01024-1

Zhang, K., Cao, C., Chu, H., Zhao, L., Zhao, J., Lee, X. (2023). Increased heat risk in wet climate induced by urban humid heat. *Nature*, *617*(7962), 738–742, https://doi.org/10.1038/s41586-023-05911-1

Zhao, L., Lee, X., Smith, R.B., Oleson, K. (2014). Strong contributions of local background climate to urban heat islands. *Nature*, *511*(7508), 216–219, https://doi.org/10.1038/nature13462

Zhao, L., Oleson, K., Bou-Zeid, E., Krayenhoff, E.S., Bray, A., Zhu, Q., ... Oppenheimer, M. (2021). Global multi-model projections of local urban climates. *Nature Climate Change*, *11*(2), 152–157, https://doi.org/10.1038/s41558-020-00958-8

Zheng, Z., Zhao, L., Oleson, K.W. (2021). Large model structural uncertainty in global projections of urban heat waves. *Nature Communications*, *12*(1), 3736, https://doi.org/10.1038/s41467-021-24113-9